Enhancing the comprehension of mixed layer depth control on the Mediterranean phytoplankton phenology

Héloïse Lavigne, Fabrizio d'Ortenzio, Christophe Migon, Hervé Claustre, Pierre Testor, Maurizio Ribera d'Alcalã, Rosario Lavezza, Loïc Houpert, Louis Prieur

JOURNAL OF GEOPHYSICAL RESEARCH: OCEANS, VOL. 118, 3416–3430, doi:10.1002/jgrc.20251, 2013

Enhancing the comprehension of mixed layer depth control on the Mediterranean phytoplankton phenology

Héloïse Lavigne,[1] Fabrizio D'Ortenzio,[1] Christophe Migon,[1] Hervé Claustre,[1] Pierre Testor,[2] Maurizio Ribera d'Alcalà,[3] Rosario Lavezza,[3] Loïc Houpert,[4] and Louis Prieur[1]

Received 10 February 2013; revised 3 May 2013; accepted 22 May 2013; published 15 July 2013.

[1] Phytoplankton phenology is primarily affected by physical forcing. However, its quantification is far from being completely understood. Among the physical forcing factors, the mixed layer depth (MLD) is considered to have the strongest impact on phytoplankton dynamics, and consequently, on their phenology. The role of MLD variations in shaping the phytoplankton phenology was explored in the Mediterranean Sea, a basin displaying contrasting phenological regimes. A database of MLD estimations was merged with ocean color chlorophyll concentrations ($[Chl]_{SAT}$) to generate concomitant annual MLD and $[Chl]_{SAT}$ cycles. Several indices were calculated to quantitatively analyze these cycles. The relevance of indices summarizing the temporal difference between main characteristics of MLD and $[Chl]_{SAT}$ cycles was emphasized. As previously observed, two dominant phenological regimes coexist in the Mediterranean Sea. The first is marked by a typical spring bloom, as in temperate regions. The second displays a low seasonality and an absence of an intense $[Chl]_{SAT}$ peak as in subtropical areas. The MLD is shown to play a key role in determining the dominant phenological regime in a given area. Results also show that regions having low seasonality display concomitant MLD and $[Chl]_{SAT}$ maxima, whereas $[Chl]_{SAT}$ peaks are generally observed 30 days after MLD peaks in regions with strongest seasonality. Over the whole basin, $[Chl]_{SAT}$ increase starts 1 month after the initiation of MLD deepening. Finally, after examining the impact of MLD on light and nutrient availability for phytoplankton, mechanisms were proposed to explain the time lags between MLD and $[Chl]_{SAT}$ increase and MLD and $[Chl]_{SAT}$ maxima.

Citation: Lavigne, H., F. D'Ortenzio, C. Migon, H. Claustre, P. Testor, M. Ribera d'Alcalà, R. Lavezza, L. Houpert, and L. Prieur (2013), Enhancing the comprehension of mixed layer depth control on the Mediterranean phytoplankton phenology, *J. Geophys. Res. Oceans*, *118*, 3416–3430, doi:10.1002/jgrc.20251.

1. Introduction

[2] Characterizing the oceanic phytoplankton phenology is a critical step to identify major alterations in the functioning of oceanic ecosystems and to further connect these alterations to global or local environmental changes. As indicated in a recent review [*Ji et al*., 2010], the description of the oceanic phytoplankton phenology implies the identification (in terms of date, duration, and magnitude) of the main steps in the temporal evolution of key parameters of an ocean ecosystem (i.e., chlorophyll-a, phytoplankton species compositions, zooplankton abundances, etc.). Linking these key episodes to environmental conditions could strongly improve our capability to identify future trends in marine ecosystem dynamics.

[3] However, until recently, the lack of data hinders a broad and global analysis of phytoplankton ocean phenology, except on some areas (i.e., Hawaii Ocean Time series (HOT) and Bermuda Atlantic Time Series (BATS)) where data are available. Satellite ocean color remote sensing, generating global and repeated observations of the ocean surface chlorophyll concentration (a proxy for phytoplankton biomass) induced a fresh impetus in the study of phytoplankton phenology. Indeed, despite the limits of the ocean color data (i.e., cloud coverage, surface observation, algorithmic issues, variation in carbon to chlorophyll ratio) numerous analyses used satellite observations of surface

Additional supporting information may be found in the online version of this article.

[1]Laboratoire d'Oceanographie de Villefranche, Université Pierre et Marie Curie and CNRS, UMR 7093, Villefranche-sur-Mer, France.
[2]Laboratoire d'Oceanographie et du Climat: Expérimentations et Approches Numériques, Université Pierre et Marie Curie, Institut Pierre Simon Laplace et CNRS, UMR 7159, Paris, France.
[3]Stazione Zoologica A. Dohrn, Laboratorio di Oceanografia Biologica, Naples, Italy.
[4]Centre de Formation et de Recherche sur les Environnements Méditerranéens, Université de Perpignan Via Domicia et CNRS, UMR 5110, Perpignan, France.
[5]Laboratoire d'Oceanographie de Villefranche, Université Pierre et Marie Curie et CNRS, UMR 7093, Villefranche-sur-Mer, France.

Corresponding author: H. Lavigne, Laboratoire d'Océanographie de Villefranche, Quai de la Darse BP08, FR-06238 Villefranche sur Mer CEDEX, France. (lavigne@obs-vlfr.fr)

2169-9275/13/10.1002/jgrc.20251

chlorophyll to provide a comprehensive description of phytoplankton phenology at global or regional scales [*Platt et al*., 2009; *Demarcq et al*., 2012; *D'Ortenzio et al*., 2012; *Racault et al*., 2012].

[4] Phytoplankton open ocean phenology is driven by a complex combination of biotic and abiotic forcings. Biotic forcings, which include the zooplankton controls of the phytoplankton accumulation, as well as the species interplay and successions, are the most difficult to assess, because in situ observations are often insufficient [*Ji et al*., 2010]. Concerning abiotic factors, the mixed layer depth (MLD), which indicates on the depth reached by turbulent mixing in a recent (order of days) past [*Brainerd and Gregg*, 1995], governs both nutrient and light availability for phytoplankton [*Mann and Lazier*, 2006], and it is historically considered the main physical factor in influencing phytoplankton dynamics.

[5] The chlorophyll response to MLD variations has been then intensively studied in the past, for the most using satellite data [*Yoder et al*., 1993; *Obata et al*., 1996; *Wilson and Coles*, 2005; *Longhurst*, 2006]. The general picture indicates a separation between temperate and polar areas, characterized by a strong seasonality in MLD variations and spectacular chlorophyll increase in spring [*Obata et al*., 1996; *Wilson and Coles*, 2005], and tropical and subtropical regions, where MLD and chlorophyll seasonal cycles are less variable and covary together, an increase in chlorophyll concentration corresponding to a deepening of the MLD [*Menzel and Ryther*, 1959; *Henson et al*., 2009]. Specific studies, focused on the North Atlantic, analyzed correlations between initiation of phytoplankton accumulation and mixed layer shallowing [*Siegel et al*., 2002; *Boss and Behrenfeld*, 2010; *Behrenfeld*, 2010; *Martinez et al*., 2011], or studied interannual or regional variability in MLD, meteorological forcing, and chlorophyll response [*Dutkiewicz et al*., 2001; *Beaugrand*, 2004; *Henson et al*., 2006]. Similarly, oligotrophic tropical and subtropical gyres were specifically studied [*McClain et al*., 2004; *Behrenfeld et al*., 2006; *Polovina et al*., 2008] by cross comparing model outputs and in situ data with ocean color observations.

[6] Mediterranean Sea, which extends from 30°N to 45°N, is positioned in the transition zone between temperate and subtropical environments. The basin is characterized by low chlorophyll values (particularly in its eastern part), with the exception of some zones, in both western and eastern regions, marked by a rapid increase of chlorophyll: the Ligurian Sea, the Southern Adriatic Sea, and the Rhodes gyre area [*Bosc et al*., 2004; *Ignatiades et al*., 2009]. Recently, satellite observations [*D'Ortenzio and Ribera d'Alcalà*, 2009, hereinafter referred to as DR09] confirmed this feature and showed a coexistence within the basin of different patterns in the seasonal cycle of surface chlorophyll concentration (associated by the authors to phenological trophic regimes). The subtropical-like regime (characterized by low seasonality) dominates almost the entire Mediterranean Sea, which displays only some spots of the temperate-like regime (characterized by a strong peak of chlorophyll during spring). Mediterranean blooming areas are characterized by strong winter mixing, inducing deep MLD and an intense refueling of nutrients in the surface layers [*Gacic et al*., 2002; *Marty et al*., 2002]. The widespread oligotrophy, on the other hand, is generally explained by relatively narrow MLDs (consequence of a weak mixing in winter and of the strong heating in summer), which would prevent a sufficient refueling of nutrients to surface layers [*Napolitano et al*., 2000].

[7] Although specific analyses have been conducted at the regional scale (in particular in the Ligurian Sea, where the largest Mediterranean blooms occur [*Lévy et al*., 1998; *Chifflet et al*., 2001; *Marty et al*., 2002; *Lacroix and Grégoire*, 2002]), very few studies explored the link between the phytoplankton phenology and MLD annual variations at the basin scale [*Crispi et al*., 2002; *Lazzari et al*., 2012, *Volpe et al*., 2012]. Nevertheless, because of the coexistence of subtropical and temperate phenological regimes in a limited space and of a relatively large spectrum of MLD conditions (spanning from very shallow layers in summer to the totally homogenized water columns in the sites of deep water formation), the Mediterranean basin represents a very good system to explore and better understand the role played by MLD dynamics in controlling phytoplankton phenology.

[8] The available observations were analyzed to explore the link between the annual cycles of surface chlorophyll concentration and MLD, by comparing the dates and magnitudes of their key events. In situ data were used to estimate the MLD and satellite surface chlorophyll-a concentrations ($[Chl]_{SAT}$ hereinafter) to derive phytoplankton phenology. The available MLD and $[Chl]_{SAT}$ data were organized in a unique database and then analyzed on the basis of the Mediterranean Sea bioregionalization provided by DR09.

[9] Three analyses are presented in this paper. For each of them, annual concomitant MLD and $[Chl]_{SAT}$ time series have been computed for each DR09 bioregion, although the data used and the averaging methods vary. In the first analysis (referred to as "Climatological"), all the data available for each bioregion were used, providing a preliminary picture of the MLD and $[Chl]_{SAT}$ seasonal variations. The second analysis (referred to as "Interannual") was focused on the interannual variability, and each year was processed separately, selecting only the MLD and $[Chl]_{SAT}$ time series having no temporal gaps. In the third analysis (referred to as "Argo float"), the MLD and $[Chl]_{SAT}$ time series was analyzed along the track of available Argo floats to verify to which extent the impact of the spatiotemporal averaging processes might affect the reconstruction.

[10] A set of indices was introduced to quantitatively assess the link between MLD and $[Chl]_{SAT}$ time series and the trends among those indices have been examined and discussed. Finally, a quantitative parameterization was developed to assess the relative role of light and nutrients in determining $[Chl]_{SAT}$ variations in the Mediterranean areas and to partially explain the differences observed in the trophic regimes. For this, a data set of Mediterranean nitrate profiles was assembled and used for statistical analysis on the relative position of MLD observations compared with the nitracline depths and the crititical depths [*Sverdrup*, 1953].

2. Data and Methods

2.1. Mixed Layer Depth

[11] The database that was used to evaluate MLD was composed of temperature and salinity profiles initially

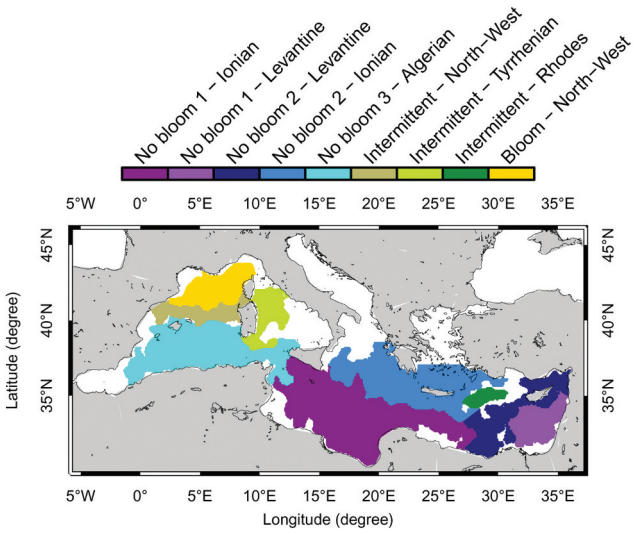

Figure 1. Spatial distribution of DR09 bioregions, redrawn for the purpose of the present analysis. See text section 2.4 for details about the modifications.

gathered to evaluate the climatological MLD in the basin (covering the 1972–2004 period [*D'Ortenzio et al*., 2005; *D'Ortenzio and Prieur*, 2010]) and merged to profiles collected during the 2004–2010 period (http://www.coriolis.eu.org/). The spatial distribution of the 72,186 available profiles is homogenous over the whole basin, although some areas are less well covered (i.e., South Tyrrhenian, North Ionian, and South Ionian from the Sicily strait to the Gulf of Sidra). After a quality control procedure for removing outliers (0.5% of profiles), potential density was calculated [*Fofonoff and Millard*, 1983], and profiles were linearly interpolated at 1 m depth interval. The MLD was calculated at the depth where the density difference from the surface reference (fixed at 10 m) is 0.03 kg m^{-3} [*de Boyer Montegut et al*., 2004; *D'Ortenzio et al*., 2005]. If no observation was available at 10 m, the shallowest measurement was used as the surface reference if it was above 20 m (12% of cases), otherwise MLD was not computed (5% of cases). When a density difference of 0.03 kg m^{-3} was not obtained throughout the profile, MLD was assumed to be the deepest measured depth (3.4% of profiles).

2.2. Surface Satellite Chlorophyll-a Concentration

[12] The 8-day Level 3 standard mapped images of SeaWiFS and MODIS Aqua surface chlorophyll at 9 km resolution were obtained from the NASA web site (http://oceancolor.gsfc.nasa.gov/) for the 1998–2010 period. SeaWiFS data were used preferentially to cover longer periods. However, some gaps in the SeaWiFS database exist after 2008, during which MODIS Aqua maps were used instead. In the Mediterranean Sea, a bias on $[Chl]_{SAT}$ observations obtained from the NASA standard algorithm [*O'Reilly et al*., 2000] was identified [*Claustre et al*., 2002; *D'Ortenzio et al*., 2002; *Bosc et al*., 2004; *Volpe et al*., 2007]. This bias, although relatively high, decreases with increasing chlorophyll concentrations. *Volpe et al*. [2007] indicate a bias of 92% on average, reduced to 29% for chlorophyll concentration larger than 0.4 mg m^{-3}. However, the NASA standard $[Chl]_{SAT}$ product was preferred to existing regional algorithms, because focus was given to the relative changes in $[Chl]_{SAT}$ (see further) rather than to the absolute values. Moreover, the NASA standard $[Chl]_{SAT}$ product allows for a better consistency between SeaWiFS and MODIS data sets [*Franz et al*., 2005], which could be relevant to avoid the introduction of any bias in the time series.

2.3. Nitrate Concentration

[13] The 5318 nitrate concentration profiles were assembled for the Mediterranean area over the 1961–2010 period. Although phosphate is generally the limiting nutrient in the Mediterranean Sea [*Ribera d'Alcalà et al*., 2003; *Pujo-Pay et al*., 2011], the number of phosphate concentration profiles available was insufficient to determine robust statistical relationships. Nitrate concentration profiles were then considered more appropriate to evaluate the nutrient availability. Data were obtained from the MEDAR-MEDATLAS [*Maillard et al*., 2005], MATER [*Maillard et al*., 2002], and SESAME (http://www.sesame-ip.eu) programs, as well as from specific cruises. A quality control procedure was applied to nitrate profiles to identify and remove outliers and spikes (16% of data points). The profiles with less than five valid data points were removed from the data set (28% of profiles). We calculated the first depth of the isocline 1 μM as a proxy of the nitracline depth (D_{nit}), similar to *Cermeño et al*. [2008]. We assumed that the nitracline separates upper nitrate-depleted waters from lower repleted waters, and, consequently, it is the first depth where nitrates are detected. In spite of the high number of D_{nit} estimations (2693 values with a resolution superior or equal to $\pm$ 25m), large areas of the basin were undersampled, particularly during winter (i.e., Tyrrhenian Sea and North Adriatic).

2.4. Bioregionalization

[14] The bioregionalization proposed by DR09 was based on a phenological criterion (i.e., the shape of the seasonal cycle of satellite-derived $[Chl]_{SAT}$). It was calculated using a k-mean cluster analysis over a 10 year SeaWiFS $[Chl]_{SAT}$ database, allowing the identification of seven dominant phenological cycles, grouped, in turn, into three more general open ocean regimes (referred to in DR09 as "Bloom", "No Bloom," and "Intermittent"). Note that for DR09 a "bloom" corresponds to a rapid accumulation of phytoplankton biomass, as it generally occurs at spring in the North Atlantic.

[15] Here, the DR09 bioregions were modified (Figure 1) as follows: (1) a 5 × 5 pixel median filter was applied to eliminate the patchiness of the DR09 and to establish well-defined continuous boundaries between two bioregions; (2) coastal bioregions of DR09, as well as zones for which the number of MLD observations was insufficient to reconstruct a seasonal cycle at 8 day resolution (i.e., Adriatic, Tyrrhenian, Aegean, Alboran, and North Ionian Seas), were excluded from the analysis; (3) bioregions originally named "Intermittent", "No Bloom 1," and "No Bloom 2" were separated into several, smaller, areas, to better account for regional specificities and to create areas without discontinuities (Figure 1).

[16] Hereafter, each bioregion is referred to by the name of the original DR09 bioregion, in which the name of the

Table 1. Description of Indices Computed From MLD and $[Chl]_{SAT}$ Time Series

Index	Description	Unit
MLD-Max	Annual maximum of MLD	meter
MLD-DateInit	Date of the initiation of the MLD increase (first time that MLD is deeper than annual median plus 5%)	days since the 177th day of the year (late June)
MLD-DateMax	Date of the annual MLD maximum	days since the 177th day of the year (late June)
CHL-Max	Annual maximum of $[Chl]_{SAT}$	mg m^{-3}
CHL-DateInit	Date of the initiation of the $[Chl]_{SAT}$ increase (first time that $[Chl]_{SAT}$ exceeds the annual median plus 5%)	days since the 177th day of the year (late June)
CHL-Datemax	Date of the annual $[Chl]_{SAT}$ maximum	days since the 177th day of the year (late June)
DeltaInit	CHL-DateInit minus MLD-DateInit	days
DeltaMax	CHL-DateMax minus MLD-DateMax	days
Corr	Spearman rank coefficient correlation between annual MLD and $[Chl]_{SAT}$ time series	dimensionless

trophic regime (i.e., "Bloom", "No Bloom," or "Intermittent") appears clearly, and by a geographical indication.

2.5. $[Chl]_{SAT}$ and MLD Time Series

[17] Considering the new spatial bioregionalization, a multiscale approach was carried out and three different spatiotemporal scales were analyzed separately. In the "Climatological" analysis, for each bioregion, a spatial average of all the MLD and $[Chl]_{SAT}$ observations available was carried out. The resulting time series were binned at an 8 day temporal resolution. The MLD and $[Chl]_{SAT}$ databases do not rigorously cover the same period (i.e., 1972–2012 for MLD and 1998–2010 for $[Chl]_{SAT}$), although they provide a general view of the first-order annual variations of the two parameters.

[18] In the "Interannual" analysis, we processed each year separately. For each bioregion, an interannual time series for MLD and $[Chl]_{SAT}$ was generated by averaging the available data over an 8 day temporal resolution. The decadal time series were separated into annual units centered on winter months (i.e., ranging from the 177th day of year n, to the 176th day of year $n+1$). We retained only the years comprising more than 38 (out of 46) MLD and $[Chl]_{SAT}$ pairs.

[19] In the "Argo float" analysis, we extracted from the MLD data set all the observations obtained from Argo floats. For each Argo profile, the satellite image that matched the date of the profile was selected and the corresponding $[Chl]_{SAT}$ over a $0.3^\circ \times 0.3^\circ$ box centered on the geographical position of the profile was extracted and averaged. Data from 99 different floats were used. Using the same procedure as for the "Interannual" analysis, the Argo $[Chl]_{SAT}$ and MLD time series lasting several years were split into annual $[Chl]_{SAT}$ and MLD series. Only complete or near-complete (starting in August or ending in May) series were retained generating 77 annual time series. To compare the "Argo float" analysis to "Climatological" and "Interannual" analyses, we assigned a bioregion to each time series on the basis of its geographical position at the time of the $[Chl]_{SAT}$ maximum. Sixty time series were assigned to one of the nine bioregions identified on Figure 1. The 17 remaining time series were not analyzed.

2.6. Indices for Characterizing $[Chl]_{SAT}$ and MLD Time Series

[20] The phenological and MLD indices calculated on $[Chl]_{SAT}$ and MLD time series are summarized in Table 1. The annual MLD and $[Chl]_{SAT}$ maxima ("Max" in Tables 2–4) were computed on each time series, as well as the date of annual maxima ("DateMax") and the date of the beginning of the MLD and $[Chl]_{SAT}$ increase ("DateInit"). After *Siegel et al*. [2002], DateInit was calculated as the first day of the year (starting in July), when $[Chl]_{SAT}$ (or MLD) exceeds the annual median plus 5%. The Spearman rank correlation ("Corr" in Tables 2–4) was computed over annual time series between MLD and $[Chl]_{SAT}$. DeltaMax (DeltaInit) indicates the time difference in days between the MLD and $[Chl]_{SAT}$ DateMax (DateInit). A positive DeltaMax (DeltaInit) index means that MLD-DateMax (MLD-

Table 2. Indices for the "Climatological" Analysis

	MLD			$[Chl]_{SAT}$			MLD/$[Chl]_{SAT}$		
Bioregion	Max	DateInit	DateMax	Max	DateInit	DateMax	DeltaInit	DeltaMax	Corr
Bloom North-West	**185**	**132 (Nov.)**	**236 (Feb.)**	**0.99**	**180 (Dec.)**	**284 (Apr.)**	**48**	**48**	**0.51**
Intermittent North-West	97	132 (Nov.)	260 (Mar.)	0.60	164 (Dec.)	268(Mar.)	32	8	0.70
Intermittent Tyrrhenian	117	132 (Nov.)	228 (Feb.)	0.42	156 (Nov.)	252 (Mar.)	24	24	0.69
Intermittent Rhodes	190	132 (Nov.)	212 (Jan.)	0.28	172 (Dec.)	252 (Mar.)	40	40	0.88
Mean Intermittent	**135**	**132 (Nov.)**	**233 (Feb.)**	**0.43**	**164 (Dec.)**	**257 (Mar.)**	**32**	**24**	**0.76**
No Bloom 1 Ionian	90	132 (Nov.)	220 (Feb.)	0.22	148 (Nov.)	228 (Feb.)	16	8	0.79
No Bloom 1 Levantine	147	116 (Oct.)	228 (Feb.)	0.19	156 (Nov.)	236 (Feb.)	40	8	0.85
No Bloom 2 Ionian	90	116 (Oct.)	228 (Feb.)	0.18	156 (Nov.)	252 (Mar.)	40	24	0.79
No Bloom 2 Levantine	115	124 (Oct.)	260 (Mar.)	0.21	164 (Dec.)	244 (Feb.)	40	−16	0.87
No Bloom 3 Algerian	50	124 (Oct.)	228 (Feb.)	0.49	140 (Nov.)	228 (Feb.)	16	0	0.79
Mean No Bloom	**99**	**122 (Oct.)**	**233 (Feb.)**	**0.26**	**152 (Nov.)**	**238 (Feb.)**	**30**	**5**	**0.82**

Table 3. Indices for the "Interannual" Analysis[a]

	MLD			$[Chl]_{SAT}$			MLD/$[Chl]_{SAT}$			
Bioregion	Max	DateInit	DateMax	Max	DateInit	DateMax	DeltaInit	DeltaMax	Corr	Number of Years[b]
Bloom North-West	**368**	**138 (Nov.)**	**255 (Mar.)**	**1.44**	**152 (Nov.)**	**286 (Apr.)**	**14**	**31**	**0.50**	**5**
Intermittent North-West	251	92 (Sep.)	248 (Mar.)	0.93	144 (Nov.)	272 (Mar.)	52	24	0.68	2
Intermittent Tyrrhenian	160	148 (Nov.)	236 (Feb.)	0.26	148 (Nov.)	252 (Mar.)	0	16	0.78	1
Intermittent Rhodes	188	108 (Oct.)	228 (Feb.)	0.48	156 (Nov.)	276 (Apr.)	48	48	0.61	1
Mean Intermittent	**212**	**110 (Oct.)**	**240 (Feb.)**	**0.65**	**148 (Nov.)**	**268 (Mar.)**	**38**	**28**	**0.69**	**4**
No Bloom 1 Ionian	108	117 (Oct.)	225 (Feb.)	0.25	136 (Nov.)	236 (Feb.)	17	11	0.81	6
No Bloom 1 Levantine	160	118 (Oct.)	236 (Feb.)	0.22	138 (Nov.)	234 (Feb.)	21	−2	0.76	5
No Bloom 2 Ionian	174	111 (Oct.)	241 (Feb.)	0.25	140 (Nov.)	235 (Feb.)	29	−6	0.80	7
No Bloom 2 Levantine	150	113(Oct.)	238 (Feb.)	0.23	140 (Nov.)	246 (Feb.)	27	8	0.74	7
No Bloom 3 Algerian	70	102 (Oct.)	222 (Feb.)	0.69	132 (Nov.)	204 (Feb.)	30	−18	0.67	5
Mean No Bloom	**136**	**112 (Oct.)**	**233 (Feb.)**	**0.31**	**138 (Nov.)**	**233 (Feb.)**	**25**	**−1**	**0.76**	**30**

[a]The indices were computed separately for each available annual time series and then averaged (the annual estimations are reported in the supporting information, Table S1).
[b]"Number of Years" indicates the number of annual series available for each bioregion.

DateInit) occurs before CHL-DateMax (CHL-DateInit). Inversely, a negative DeltaMax (DeltaInit) index means that CHL-DateMax (CHL-DateInit) precedes MLD-DateMax (MLD-DateInit).

3. Results

3.1. "Climatological" Analysis

[21] The "Climatological" MLD time series (Figure 2) exhibits a similar shape for all bioregions, marked by a progressive increase during winter and a maximum in late winter, followed by a steep decrease in spring, and low values in summer. The values of MLD-Max (Table 2) are close, except for the "Bloom North-West" and the "Intermittent Rhodes" bioregions, which show the greatest depths. The scattering of single MLD values (i.e., the red points in Figure 2), is high for the "Bloom" and "Intermittent" regimes. In particular, in the "Bloom North-West" bioregion, very deep MLDs could episodically be observed in winter (Figure 2). Although MLD-DateMax values range between day 212 (January, "Intermittent Rhodes") and 260 (March, "Intermittent North-West" and "No Bloom 2 Levantine"), most of the bioregions exhibit a MLD-DateMax around day 230 (i.e., February). The MLD-DateInit values are also similar among bioregions (October/early November).

[22] The $[Chl]_{SAT}$ "Climatological" seasonal cycles calculated for each bioregion (Figure 2) are close to those described by DR09 (bioregions used here derived from the DR09 ones). The three main regimes described by DR09 ("Bloom", "Intermittent," and "No Bloom") are confirmed, as well as their phenological characteristics. For the "Bloom" and "Intermittent" regimes, $[Chl]_{SAT}$ slightly increases in winter. Then, for the "Bloom", $[Chl]_{SAT}$ exhibits a sharp increase in late winter/early spring, reaching the maximum value in spring. For the "Intermittent" regime, a second and less intense increase is observed in late winter. The "No Bloom" regime displays another pattern, characterized by low values most of the year, and a slight increase during winter months. The differences between regimes are reflected in the CHL-Max and CHL-DateMax (Table 2). CHL-Max shows a west-east gradient (highest values for the "Bloom North-West" bioregion) and CHL-DateMax changes with biological regime (CHL-DateMax is in April for the "Bloom," in March for the "Intermittent" and in February/early March for the "No Bloom" regime). Differences are also observed for

Table 4. Indices for the "Argo Float" Analysis[a]

	MLD			$[Chl]_{SAT}$			MLD/$[Chl]_{SAT}$			
Bioregion	Max	DateInit	DateMax	Max	DateInit	DateMax	DeltaInit	DeltaMax	Corr	Number of Years[b]
Bloom North-West	**980**	**107 (Oct.)**	**252 (Mar.)**	**1.86**	**133 (Nov.)**	**279 (Apr.)**	**26**	**27**	**0.14**	**3**
Intermittent North-West	303	87 (Sep.)	235 (Feb.)	1.03	128 (Nov.)	249 (Mar.)	41	14	0.56	7
Intermittent Rhodes	442	129 (Nov.)	243 (Feb.)	0.39	138 (Nov.)	260 (Mar.)	9	17	0.73	4
Intermittent Tyrrhenian	102	126 (Oct.)	242 (Feb.)	0.48	151 (Nov.)	267 (Mar.)	25	25	0.30	1
Mean Intermittent	**282**	**114 (Oct.)**	**240 (Feb.)**	**0.63**	**139 (Nov.)**	**259 (Mar.)**	**25**	**19**	**0.53**	**12**
No Bloom 1 Ionian	133	107 (Oct.)	239 (Feb.)	0.21	129 (Nov.)	224 (Feb.)	22	−14	0.68	16
No Bloom 1 Levantine	197	104 (Oct.)	241 (Feb.)	0.20	144 (Nov.)	234 (Feb.)	40	−7	0.70	8
No Bloom 2 Ionian	188	106 (Oct.)	234 (Feb.)	0.24	140 (Nov.)	243 (Feb.)	34	9	0.67	7
No Bloom 2 Levantine	198	99 (Oct.)	246 (Feb.)	0.26	148 (Nov.)	260 (Mar.)	48	13	0.62	6
No Bloom 3 Algerian	105	86 (Sep.)	214 (Jan.)	0.93	139 (Nov.)	219 (Jan.)	53	5	0.54	8
Mean No Bloom	**164**	**100 (Oct.)**	**235 (Feb.)**	**0.37**	**140 (Nov.)**	**236 (Feb.)**	**39**	**1**	**0.64**	**45**

[a]The indices were computed separately for each available "Argo float" time series and then averaged.
[b]"Number of Years" indicates the number of annual series available for each bioregion.

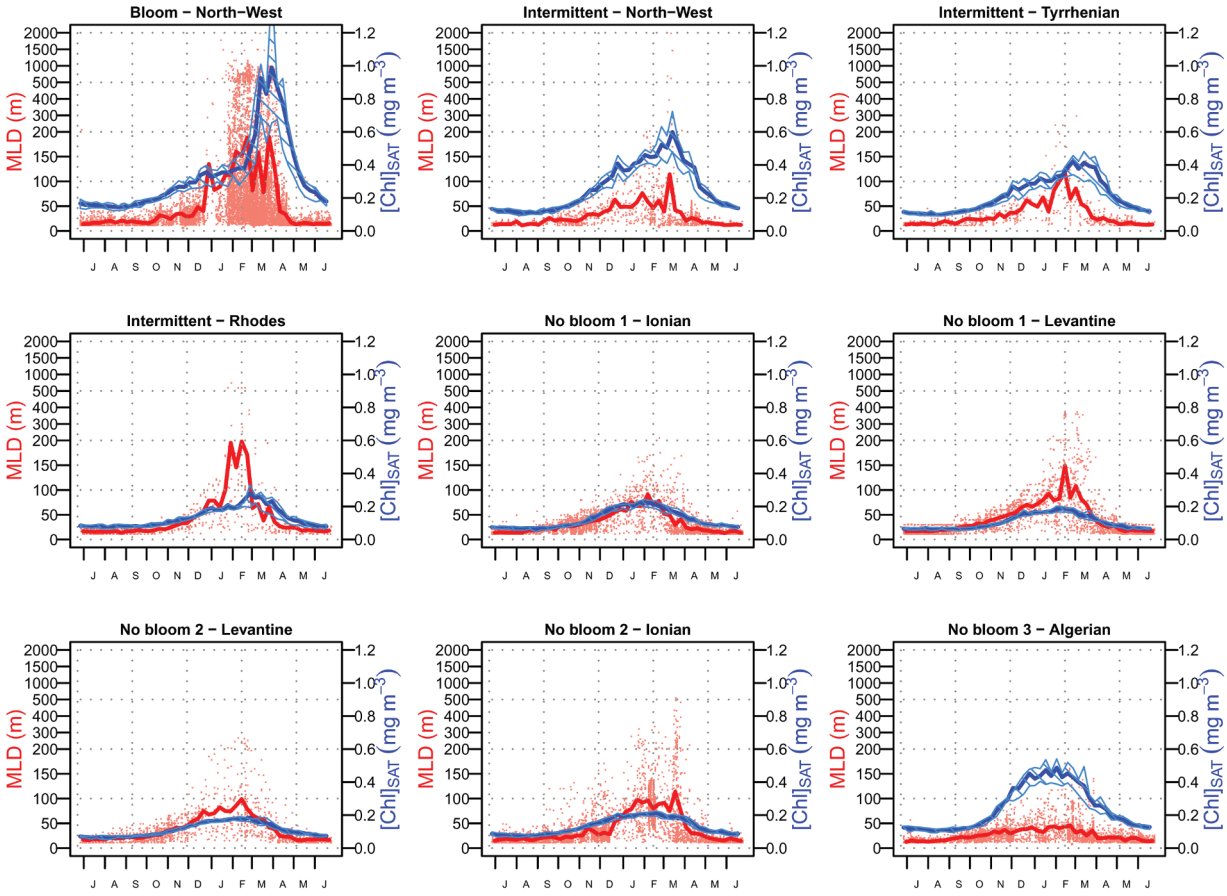

Figure 2. Climatological distribution of MLD (red solid line) and $[Chl]_{SAT}$ (blue solid line) with its standard deviation range (blue hatched zone), at 8 day resolution. All the available MLD observations are depicted with light red dots. Note that the MLD scale is not linear.

CHL-DateInit (Table 2), which is observed around day 180 for the "Bloom" regime, day 164 for the "Intermittent" and day 152 for the "No Bloom."

[23] The $[Chl]_{SAT}$ and MLD time series are generally strongly correlated (Corr in Table 2). Only the "Bloom" regime shows a value of about 0.5, which is likely caused by the time lag between MLD-Max and CHL-Max. For the "Bloom" regime, DeltaMax value is 48 days, whereas for the "Intermittent" it is 24 days and for the "No Bloom" regime it is around zero (with the notable exception of the "No Bloom 2 Ionian" bioregion). The DeltaInit values (Table 2) are, conversely, much more similar in the various bioregions (i.e., around 30 days), with, again, an exception for the "Bloom" regime (i.e., 48 days).

3.2. "Interannual" Analysis

[24] In the "Interannual" analysis, we mainly focused on the interannual patterns and on their deviation from the climatology. The indices, calculated for each year, are reported in the supporting information (Table S1) and the average of the single annual estimations is in Table 3. Figure 3 shows the available seasonal cycles for both $[Chl]_{SAT}$ and MLD, for each bioregions.

[25] For the "Bloom North-West" bioregion (five annual cycles), the shapes of the seasonal evolution of MLD and $[Chl]_{SAT}$ vary from year to year, although the succession of the main events (i.e., MLD deepening and $[Chl]_{SAT}$ increase and decay) is repeated (Figure 3a). However, the cycle for the 2006/2007 year is anomalous, resembling a typical "No Bloom" condition. For the "Intermittent" and "No Bloom" bioregions, the shapes of the seasonal cycles appear qualitatively similar to their "Climatological" counterpart (compare Figures 2 and 3), therefore indicating a very low interannual variability. Note that, overall, the absolute values, in particular for the MLD and $[Chl]_{SAT}$ peaks, could be highly variable interannually (compare for example 2003/2004 and 2008/2009 for the "No Bloom 1 Levantine" bioregion, Figure 3d). Nevertheless, the shape and the timing of the events are relatively recurrent from year to year for all bioregions. The interannual variability can then be quantified by analyzing the time series indices defined in section 2.6.

[26] For the "Bloom North-West" bioregion, the values of DateMax and Max for both the MLD and $[Chl]_{SAT}$ parameters show high interannual variability (Table S1). The var index on Table S1 indicates the percentage difference between the individual estimations of MLD-Max (or CHL-Max) and the interannual average of MLD-Max (or CHL-Max) reported on Table 3. Averaging all the var estimations, it appears that MLD-Max shows a 55% deviation from the interannual mean, while CHL-Max shows a 16% deviation. The CHL-Max values are generally high (close

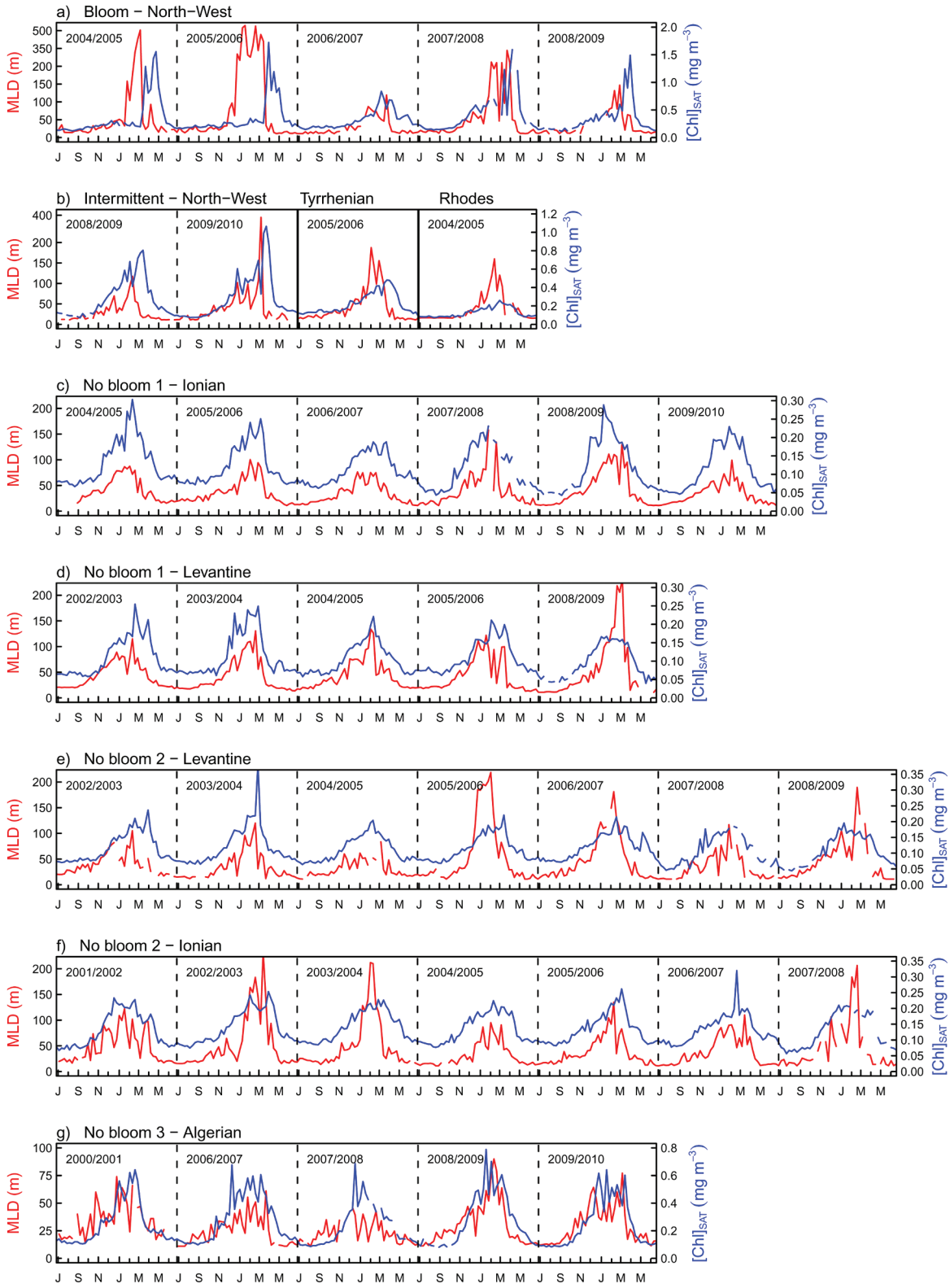

Figure 3. Interannual variations of MLD (red line) and $[Chl]_{SAT}$ (blue line). Annual periods were considered from July to June (dotted vertical lines). Note that the MLD scale is not linear.

to 1.50 mg m^{-3} for most of the years) and less variable than MLD-Max, which ranges between 119 and 523 m. In this bioregion, MLD-DateMax and CHL-DateMax range between days 212 and 276 and between days 260 and 308, respectively (Table S1). The MLD-DateInit and CHL-DateInit are less variable: the first always occurring in early November, the second observed from day 140 (late November) to 172 (early December). DeltaInit is

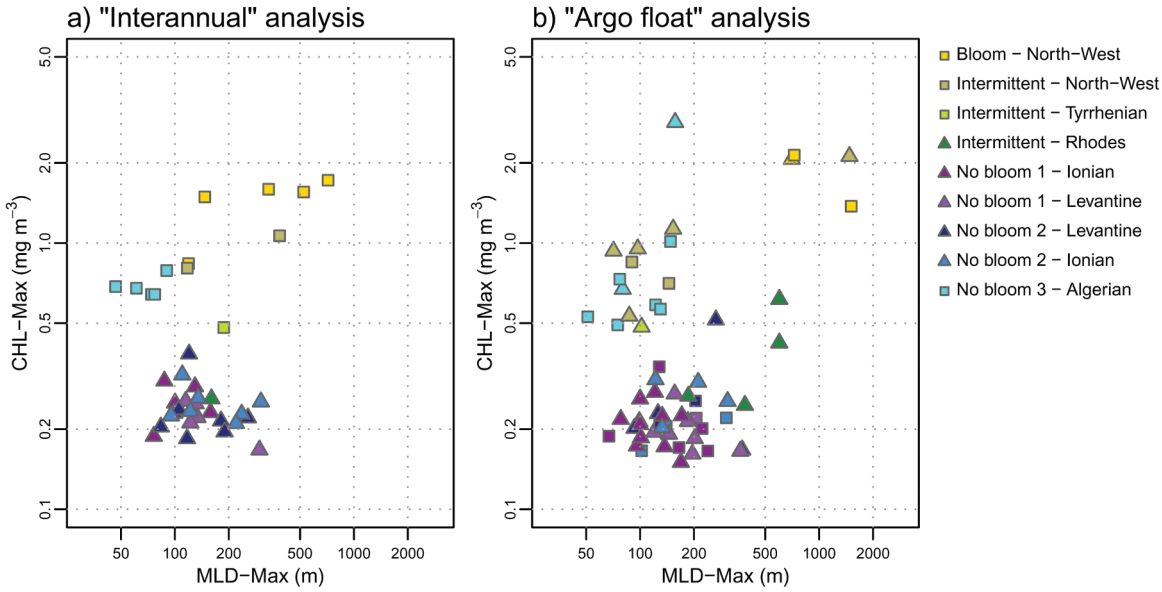

Figure 4. Scatter plot of MLD-Max versus CHL-Max. Points are derived from (a) the "Interannual" analysis and (b) "Argo float" analysis. Squares refer to points corresponding to the western Mediterranean Sea and triangles to its eastern basin.

consequently constant over the years (14 days on average, Table 3). Excluding the 2006/2007 time series, DeltaMax in this bioregion is always positive (greater than 16 days). As it is qualitatively evident from Figure 3a, the 2006/2007 cycle strongly diverges from the others. During this year, the lowest MLD-Max and CHL-Max were obtained and DeltaMax was negative (i.e., −16 days, Table S1). *Bernardello et al*. [2012] observed a similar pattern for phytoplankton biomass dynamics during winter 2007 and ascribed it to specific meteorological factors characterized by an abnormally low wind stress and by heat fluxes that were only slightly negative compared to other winters over the 2002–2010 period.

[27] For the "Intermittent" regimes, the lack of MLD data allows to describe only four annual cycles, for three different bioregions (Figure 3b and Table S1). The MLD-Max and CHL-Max present important interannual variability ("Intermittent North-West" bioregion) as well as within bioregions. Conversely, the temporal indices (with the exception of MLD-DateInit) are weakly variable interannually (Table S1). In particular, DeltaMax is very stable (on average 32 days, Table 3) and seems to be constant for the three different "Intermittent" bioregions.

[28] For the "No Bloom" bioregions, 30 annual cycles were obtained (Figures 3c–3g and Table 3). The MLD-DateMax and CHL-DateMax values exhibit interannual variability, ranging between day 148 (November) and 168 (March) and between day 172 (December) and 284 (April), respectively. In consequence, DeltaMax also displays important variability with values spanning between −104 and +88 days (Table S1). Considering the shape of the seasonal MLD and $[Chl]_{SAT}$ evolution, the strong variability of the DateMax index is, however, not surprising. Indeed, both MLD and $[Chl]_{SAT}$ cycles rarely exhibit a clear peak, most of the cycles displaying only a winter plateau (Figure 3). However, when interannual estimations are averaged for "No Bloom" bioregions (Table 3), DeltaMax shows more stable values, generally close to zero. Phasing between MLD and $[Chl]_{SAT}$ cycles is confirmed more quantitatively by the high values of the Corr index (0.76 on average and always superior to 0.61). The values for the DateInit indices present a low variability between years and bioregions, with most of the values observed around days 112 (October) for MLD-DateInit and around day 138 (November) for CHL-DateInit. DeltaInit is also fairly stable (the average is +25 days, Table 3). Finally, MLD-Max displays higher interannual variability than CHL-Max. MLD-Max shows 30% average deviation from the interannual mean while it is only 12% for CHL-Max (see var index on Table S1).

[29] Comparing the indices of "Interannual" and "Climatological" analysis (Tables 2 and 3), differences are generally small for temporal indices. Some exceptions are, however, evident. In the "Bloom North-West" bioregion, DeltaInit and DeltaMax of the "Interannual" analysis are reduced to 14 and 31 days, respectively. Values of MLD-Max and CHL-Max indices in the "Interannual" analysis are generally lower than in the "Climatological" analysis. This is true for all the bioregions, though particularly evident in the "Bloom North-West" bioregion. Finally, for "Intermittent" and "No Bloom" bioregions Corr is smaller in the "Interannual" analysis than in the "Climatological" analysis.

[30] To complete the analysis, the combined distribution of CHL-Max and MLD-Max were compared (Figure 4a). Results show that points tend to aggregate by bioregion. A separation between western (squares on Figure 4a) and eastern bioregions (triangles on Figure 4a) is also observed. Western bioregions generally display higher CHL-Max values than the eastern ones.

3.3. "Argo float" Analysis

[31] In the "Argo float" analysis, Argo MLD and $[Chl]_{SAT}$ specific time series were compared with the climatology to determine the characteristics which are

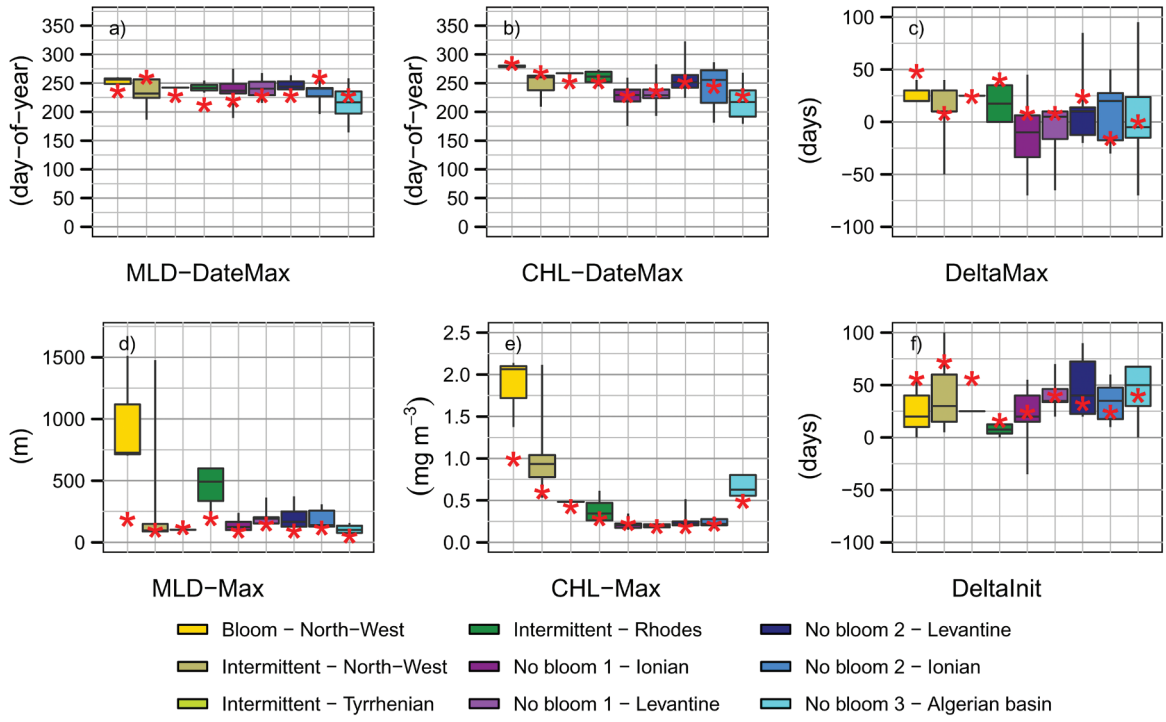

Figure 5. Distribution of the values computed from the "Argo float" time series for six selected indices: (a) MLD-DateMax, (b) CHL-DateMax, (c) DeltaMax, (d) MLD-Max, (e) CHL-Max, and (f) DeltaInit. The distributions in the index estimations are represented with box plots, for each bioregion separately (color refers to bioregion). Note that whiskers of box plots range from minimum to maximum estimations and colored boxes from the first to the third quartile. The red stars superimposed to box plots indicate the position of climatological estimations that are summarized in Table 2. For MLD-DateMax and CHL-DateMax, "day-of-year" is the day-of-year number starting from the 177th day of the calendar year (i.e., 26 June).

maintained (or not). A summary of indices computed on each of the 60 available annual "Argo float" time series is reported in Table 4. The scattering of some indices with respect to the "Climatological" analysis is represented on Figure 5. The scatter plot of MLD-Max versus CHL-Max is shown in Figure 4b, for sake of comparison with the similar plot of the "Interannual" analysis (Figure 4a).

[32] When the "Argo float" MLD-Max and CHL-Max are compared (Figure 4b), the resulting patterns are fairly similar to those observed in the "Interannual" analysis (Figure 4a). Nevertheless, some differences appear. Points are more scattered in the "Argo float" analysis than in "Interannual" analysis. The difference between eastern and western bioregions is also obtained in the "Argo floats" analysis. However, the distribution of western (squares on Figure 4b) and eastern (triangles on Figure 4b) points present similarities, not evident in the "Interannual" analysis. For both eastern and western bioregions, most of the points characterized by low CHL-Max and low MLD-Max belong to the "No Bloom" or "Intermittent" bioregions. Points marked by high MLD-Max and high CHL-Max belong to the "Bloom North-West" and "Intermittent North-West" bioregions (western basin) or to "Intermittent Rhodes" bioregion (eastern basin). For the western points (squares on Figure 4b) an important gap is observed in the distribution of MLD-Max values. There is no observation between 200 and 500 m.

[33] Box plots in Figure 5 represent, for each bioregion (differentiated with color), the distribution of values computed on "Argo float" MLD and $[Chl]_{SAT}$ time series for six selected indices. To compare the "Argo float" distribution for the selected indices with their climatological value (available on Table 2), the climatological estimations are superimposed to box plots (red stars on Figure 5). From Table 4 and Figure 5f, it appears that DeltaInit values are very close to their "Climatological" counterpart (except for the "Bloom North-West", "Intermittent North-West," and "Intermittent Tyrrhenian" bioregions). DateInit values for both MLD and $[Chl]_{SAT}$ parameters are advanced, by 21 days on average, in the "Argo float" analysis compared with the "Climatological" analysis (compare Tables 4 and 2). The largest differences were observed for CHL-DateInit in the "Bloom North-West" bioregion (47 days). DateMax and DeltaMax values are generally unchanged between the "Argo float" and "Climatological" analyses (except again for "Bloom North-West" bioregion: MLD-DateMax is delayed by 15 days compared to the "Climatological" analysis, resulting in a shorter DeltaMax, Figures 5a–5c). In all bioregions (except "Intermittent Tyrrhenian"), the MLD-Max of "Climatological" analysis are lower than in the "Argo float" analysis (Figure 5d). This effect is particularly strong in the "Bloom North-West" bioregion where a factor of 5 is observed. Similarly, CHL-Max values are higher in the "Argo float" analysis than in

the "Climatological" (Figure 5e). This trend is especially evident in bioregions having relatively high $[Chl]_{SAT}$ values (i.e., "Bloom North-West", "Intermittent" bioregions, and "No Bloom 3 Algerian Basin"). Finally, the Corr index is systematically lower in the "Argo float" than in the "Climatological" analysis.

4. Discussion

4.1. General Patterns of Mediterranean MLD Dynamic and $[Chl]_{SAT}$ Phenology

[34] Phytoplankton phenology and seasonal cycle of MLD were simultaneously analyzed using an in situ database of MLD and satellite ocean color $[Chl]_{SAT}$ data. Available data were merged into bioregions (obtained from DR09), which are large oceanic zones considered to share similar patterns of the seasonal $[Chl]_{SAT}$ evolution. The resulting $[Chl]_{SAT}$ and MLD time series averaged over bioregions are consistent with seasonal cycles previously observed in the Mediterranean Sea [*Bosc et al*., 2004; *D'Ortenzio et al*., 2005; DR09; *D'Ortenzio and Prieur*, 2010]. The approach using bioregions therefore appears to be a pertinent manner to identify patterns in large oceanic data sets.

[35] While searching for relationships between external forcing and phytoplankton phenological response, the use of $[Chl]_{SAT}$ to represent phytoplankton biomass presents two main limitations. As the chlorophyll to carbon ratio exhibits a variability that is not easy to parameterize [*Cullen*, 1982; *Geider et al*., 1997; *Behrenfeld et al*., 2005], the interpretation of the $[Chl]_{SAT}$ time series as biomass seasonal cycles requires particular caution. Consequently, a clear distinction between chlorophyll concentration and biomass was made, in order to avoid any ambiguity. Moreover, assuming constant chlorophyll to carbon ratio, variations in surface $[Chl]_{SAT}$ do not always represent changes in phytoplankton growth rate. This could be particularly relevant when deep turbulent mixing dilutes phytoplankton cells, yielding a $[Chl]_{SAT}$ decrease at the surface, while phytoplankton growth rate may be constant or positive (see *Behrenfeld* [2010] for an exhaustive discussion). However, as MLD does not necessarily match with the mixing layer depth (the depth reached by active turbulence at the time of observation [*Brainerd and Gregg*, 1995], the limitation of the $[Chl]_{SAT}$ as a proxy of biomass was accounted for and, contrarily to *Behrenfeld* [2010], the integrated contents were not used. In addition, using $[Chl]_{SAT}$ instead of integrated chlorophyll contents does not introduce an important bias in the visualization of the seasonal pattern of the phytoplankton dynamics [*Boss and Behrenfeld*, 2010].

[36] Keeping in mind the above limitations, a set of indices were introduced to describe the seasonal cycles of MLD and $[Chl]_{SAT}$. Some of them were previously used in the literature (i.e., CHL-DateInit [*Siegel et al*., 2002; *Henson et al*., 2006], Corr [*Henson et al*., 2009], CHL-DateMax and CHL-Max [*Racault et al*., 2012], MLD-DateMax, MLD-Max [*de Boyer Montégut et al*., 2004; *Carton et al*., 2008], while others were developed specifically in this paper (i.e., DeltaMax, DeltaInit). The analysis of the indices confirmed some aspects of the Mediterranean MLD and $[Chl]_{SAT}$ behaviors already observed, though newly introduced elements require further analysis:

[37] (1) It can be confirmed that eastern and western basins are not equivalent regarding the MLD and $[Chl]_{SAT}$ range of values [*Moutin and Raimbault*, 2002; *Bosc et al*., 2004; *D'Ortenzio et al*., 2005]. Higher CHL-Max values and lower MLD-Max values were observed in the western bioregions than in the eastern ones (with the exception of the "Bloom North-West" region that displayed the highest MLD-Max values).

[38] (2) As previously observed [*Napolitano et al*., 2000; *Gacic et al*., 2002; *Marty et al*., 2002], this study confirmed that, in the Mediterranean, high $[Chl]_{SAT}$ values are observed in bioregions characterized by deep MLD. Indeed, CHL-Max and MLD-Max present a positive trend when passing from "No Bloom" to "Intermittent" and finally to "Bloom" bioregions. The general principle: "deeper MLD implies higher $[Chl]_{SAT}$" therefore seems to be roughly confirmed at the scale of Mediterranean subbasins. However, within a same bioregion, no positive relationship between MLD-Max and CHL-Max was observed. More specifically, the "Interannual" and "Argo float" analyses showed that, inside "Bloom" or "No Bloom" bioregions, the MLD-Max observations are generally highly variable whereas CHL-Max observations remain stable (Figures 4 and Table S1). This result suggests that although the intensity of winter mixing appears to have an impact on the general dynamics of phytoplankton phenology (i.e., "Bloom" or "No Bloom"), other parameters than solely MLD-Max determines the value of CHL-Max.

[39] The "Interannual" and "Argo float" analyses showed that high interannual and spatial variabilities characterize "Intermittent", and, to a lesser extent, "Bloom" bioregions (as already hypothesized by DR09). The specific behavior of the cycle 2006/2007 in the "Bloom North-West" bioregion (Figure 3a) clearly illustrates the impact of the interannual variability. In these bioregions, $[Chl]_{SAT}$ annual dynamics may oscillate between typical "Bloom" and "No Bloom" dynamics, depending on the interannual variability of meteorological factors (i.e., wind stress and heat fluxes). In the future, if climate change tends to reduce wind stress and weaken winter heat fluxes [*Somot et al*., 2006], the occurrence of the "No Bloom" dynamics, compared to the "Bloom" dynamics, may then increase.

[40] All the above observations have already been identified for Mediterranean Sea in the past [e.g., *Bernardello et al*., 2012; *Lazzari et al*., 2012; *Volpe et al*., 2012]. However, the previous studies focused mostly on the absolute values of the phytoplankton biomass and MLD peaks (i.e., our MLD-Max and CHL-Max indices), neglecting the temporal dimension. In particular, the analysis of the temporal differences between the dates of major events of the MLD and phytoplankton biomass time series (our DeltaMax and DeltaInit indices) has never yet been addressed before in the Mediterranean Sea. In fact, we demonstrated that the different averaging procedures (i.e., "Climatological," "Interannual," and "Argo floats" analysis) affect the values of our Max indices. On the other hand, we demonstrated that delta indices appear less affected by the averaging procedures. Therefore, in the following, we will focus on these two indices.

[41] Because the DeltaInit index does not relevantly change with the analysis (i.e., "Climatological," "Interannual," or "Argo float"), we assumed that it reflects a realistic pattern of the MLD and $[Chl]_{SAT}$ series. In the different Mediterranean bioregions, DeltaInit values cluster around 30 days, which indicates that the annual increase of $[Chl]_{SAT}$ follows the seasonal deepening of the MLD. Interestingly, the $[Chl]_{SAT}$ increase always occurs in November/early December in the whole basin, though the date of deepening of the MLD is more variable (MLD-DateInit spans between September and November). This apparent contradiction could be solved by evoking the spatial distribution of nutrients in the basin and its interplay with the amplitude of the mixing (i.e., MLD-Max). This will be discussed further.

[42] Similar to the DeltaInit, the DeltaMax index appears to be independent of the averaging method used to evaluate it. With the noticeable exception of the "Bloom North-West" bioregion, no major difference was observed between the estimations of DeltaMax in the "Climatological," "Interannual," and "Argo float" analyses, which indicates that DeltaMax represents a realistic pattern of the MLD and $[Chl]_{SAT}$ series in the Mediterranean. For the "Bloom North-West" bioregion, the DeltaMax at "Climatological" scale (48 days) strongly differs from the "Interannual" and "Argo float" estimations (31 and 27 days, respectively). This time lag of 48 days between MLD-Max and CHL-Max appears too large to represent a realistic phytoplankton response to MLD variations. It is assumed to be an artifact due to the averaging procedure, and, in the further discussion on the "Bloom" bioregions, we will only consider the DeltaMax estimations derived from the "Interannual" and "Argo float" analyses. A clear distinction between the "Bloom" and "Intermittent" and the "No Bloom" bioregions for the DeltaMax index emerges from our analysis when we consider averaged values over bioregions. In the "No Bloom" bioregions, despite important individual variability in the "Interannual" and "Argo float" analyses, the two annual maxima (MLD and $[Chl]_{SAT}$) coincide temporally, occurring in most cases in February. For the "Bloom" and, to a lesser extent, for the "Intermittent" bioregions, the $[Chl]_{SAT}$ maxima are delayed respect to the MLD peaks. The variability of the DeltaMax index among the bioregions is primarily induced by CHL-DateMax, as the MLD-DateMax is almost constantly observed in February. This is evident in the "Argo floats" analysis, where CHL-DateMax exhibits a significant delay (student test 95%) when passing from "No Bloom", to "Intermittent" and to "Bloom" regime (Figure 5). In addition, the largest values of DeltaMax are generally associated to the highest values of CHL-Max and MLD-Max observed in the Mediterranean (i.e., in the "Bloom" and the "Intermittent" regions), although, as for the positive relationship between MLD-Max and CHL-Max (see above), this result only seems true at the scale of the Mediterranean basin. Overall, we demonstrated that the temporal difference between MLD-Max and CHL-Max (i.e., the index DeltaMax) is an important feature of MLD and $[Chl]_{SAT}$ time series that differentiates the two dominant trophic regimes that coexist in the Mediterranean Sea.

[43] In summary, the "Intermittent" bioregions, displaying typical "Bloom" like and "No Bloom" like time series, could be considered as hinge regions between "Bloom" and "No Bloom" bioregions and, therefore, would be key areas in the Mediterranean Sea. However, as we did not detect a clear specific pattern representing "Intermittent" MLD and $[Chl]_{SAT}$ time series, the next discussion will focus only on "Bloom" and "No Bloom" bioregions. In the "No Bloom" bioregions the MLD seasonal increase occurs 1 month before $[Chl]_{SAT}$ seasonal increase, whereas MLD and $[Chl]_{SAT}$ maxima are concomitant. The $[Chl]_{SAT}$ peaks, however, remain relatively low, and they are independent of the amplitude of the MLD-Max. In the "Bloom" bioregion, we similarly observe a delay in the seasonal $[Chl]_{SAT}$ increase compared to the MLD increase. Additionally, in most cases, a time lag of about 30 days was observed between the two peaks (MLD peak occurring before $[Chl]_{SAT}$ peak).

[44] As already introduced, MLD has an impact on the phytoplankton phenology mostly because it controls the availability of nutrients and light. Although solar radiation is relatively high throughout the year in temperate and subtropical regions (as the Mediterranean), deep MLD could have a role in redistributing phytoplankton through the water column. Subsequently, phytoplankton cells could spend significant periods of time outside of the illuminated depths, and its growth could therefore be affected, even in a high-nutrient environment. Consequently, it could impact on the date and the intensity of the $[Chl]_{SAT}$ events.

[45] To explain the "Bloom" and "No Bloom" DeltaInit and DeltaMax differences, an additional analysis was introduced, considering nutrients and light observations as well. The limitation of the data availability (particularly important for the nutrients) prevents a complete, basinwide analysis. Therefore, focus is put on two bioregions (i.e., "Bloom North-West" and "No Bloom 1 Ionian") considered as representative of their trophic regime.

4.2. Abiotic Factors Controlling the Mediterranean Phenological Regimes

[46] To verify how MLD controls light and nutrient availability for phytoplankton in the Mediterranean area, MLD data were concurrently analyzed with the nitracline depth (D_{nit}) and the critical depth (D_{cr}) estimations. The first was considered as a proxy of the nutricline depth, and the second as an estimator of the light limitation depth. D_{cr}, defined as the depth where integrated phytoplankton production in the layer above this depth equals integrated losses due to respiration [*Sverdrup*, 1953], was estimated using the following equation [*Siegel et al*., 2002]:

$$\frac{1}{K_{PAR} \cdot D_{cr}}\left(1 - e^{-K_{PAR}D_{cr}}\right) = \frac{I_c}{PAR} \quad (1)$$

where I_c is the irradiance for which net community production equals net community respiration (the compensation irradiance), PAR is the photosynthetically available radiation at the surface, and K_{PAR} is the PAR diffuse attenuation coefficient. Monthly climatological estimations of D_{cr} were computed, using a SeaWiFS monthly climatology of PAR and $K_{d(490)}$, transformed into K_{PAR} with *Rochford et al*. [2001] equations. As there is no consensus concerning the I_c values [*Siegel et al*., 2002], D_{cr} was computed for a range of I_c values spanning from 0.5 to 2 mol photons m^{-2} d^{-1}

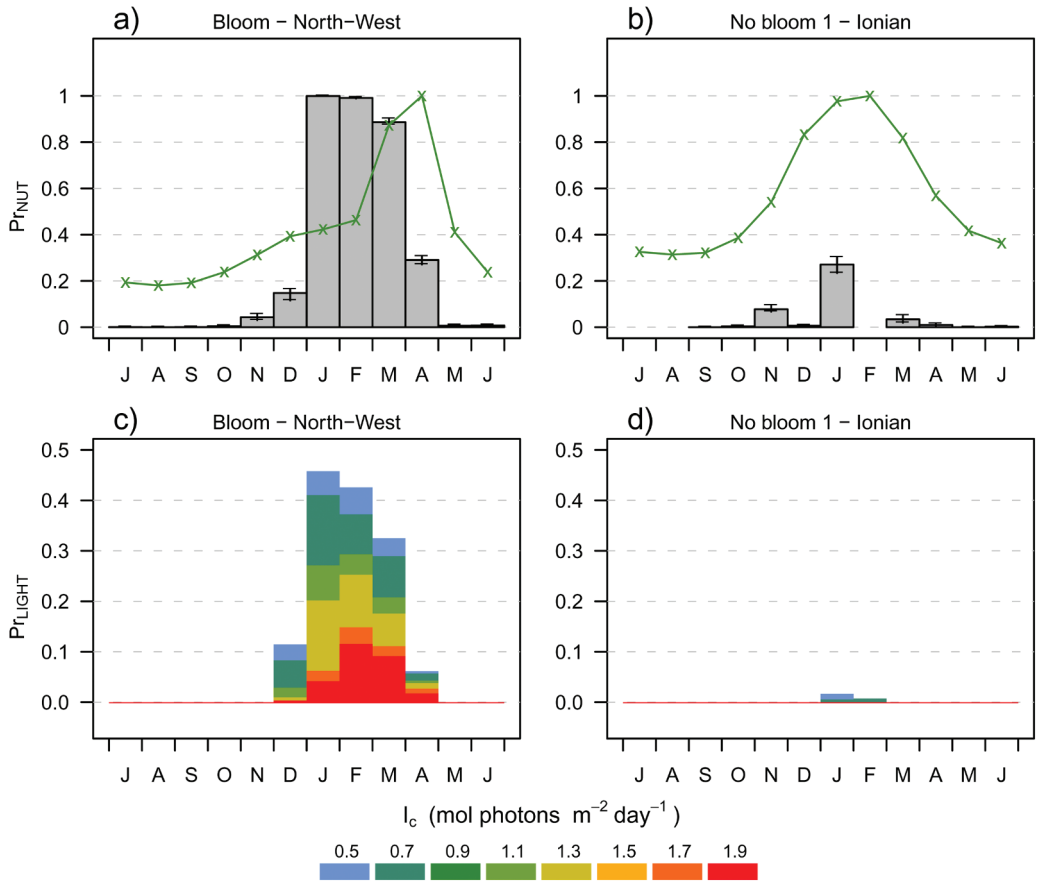

Figure 6. Monthly distribution of (a and b) P_{rNUT} (probability that MLD be deeper than nitracline depth) and (c and d) P_{rLIGHT} (probability that MLD be deeper than the critical depth) for the bioregions "Bloom North-West" and "No Bloom 1 Ionian." In Figures 6a and 6b the absence of rectangle indicates the absence of D_{nit} data, black lines indicate that P_{rNUT} is null. For P_{rNUT} estimations, confidence intervals are indicated by error bars. To provide a confidence interval around the P_{rNUT} value, one third of MLD and D_{nit} data, randomly selected were removed from the data set and a new P_{rNUT} value was computed. This operation was repeated 100 times, the smallest and the highest values of P_{rNUT} were retained to define the confidence interval. The absence of confidence interval indicates that less than three nitracline depth observations were available to compute P_{rNUT}. Normalized climatological $[Chl]_{SAT}$ cycle is referred to with the green line. In Figures 6c and 6d, color refers to the value of I_c used to compute D_{cr}.

(I_c estimations from *Siegel et al.* [2002] range between 1 and 1.5 mol photons m^{-2} d^{-1}).

[47] Then, for each bioregion, we calculated the probabilities (P_{rNUT} and P_{rLIGHT}) that MLD is deeper than D_{nit} (equation (2)) or D_{cr} (equation (3)).

$$P_{\mathrm{rNUT}} = \frac{\sum_{i=1}^{n_{nit}} \sum_{j=1}^{n_{MLD}} f\left(D_{nit,i}, MLD_j\right)}{n_{nit} \times n_{MLD}}, \quad \text{with } f\left(D_{nit,i}, MLD_j\right) = 1 \text{ if } D_{nit,i} \le MLD_j \text{ and } 0 \text{ otherwise} \tag{2}$$

$$P_{\mathrm{rLIGHT}}(I_c) = \frac{\sum_{j=1}^{n_{MLD}} f\left(D_{cr}(I_c), MLD_j\right)}{n_{MLD}}, \quad \text{with } f\left(D_{cr}(I_c), MLD_j\right) = 1 \text{ if } D_{cr}(I_c) \le MLD_j \text{ and } 0 \text{ otherwise} \tag{3}$$

[48] In equations (2) and (3), $D_{nit,i}$ indicates the *i*th estimation of D_{nit} and MLD_j the *j*th estimation of the MLD for a given month and a given bioregion. n_{nit} and n_{MLD} are, respectively, the number of available D_{nit} observations and MLD observations. In equation (3), all the MLD observations are compared to the unique (and climatological) estimation of D_{cr}, whereas all possible combinations between MLD and D_{nit} observations are tested in equation (2). The resulting distribution of P_{rNUT} and P_{rLIGHT} for the "Bloom North-West" and "No Bloom 1 Ionian" bioregions is displayed in Figure 6.

[49] In the "Bloom North-West" bioregion, P_{rNUT} values start to be greater than zero in November, indicating that, episodically, nutrient limitation is relaxed (Figure 6a). As P_{rLIGHT} is zero, there is no light limitation for phytoplankton growth (Figure 6c). The concurrent absence of light and nutrient limitations is consistent with the initiation of $[Chl]_{SAT}$ increase that occurs in November/early December (CHL-DateInit, Tables 2–4). In January and February, P_{rNUT} is very close to 1, indicating that, during this period, MLD is permanently deeper than the nitracline depth (Figure 6a). Yet, MLD can also be shallow during this period (Figure 2), and nitrate concentration at the surface should

be permanently superior to 1 μM. During the same period, whatever the I_c value, P_{rLIGHT} is not null (ranges between 0.05 and 0.45, Figure 6c), suggesting that during deep mixed layer events, phytoplankton accumulation is prevented. During the winter period, a deficit of light would prevent the total utilization of nitrate stocks in surface layers by phytoplankton. When P_{rLIGHT} starts to decrease (in March), P_{rNUT} is still high (about 0.9), both limiting conditions are relaxed, and a sharp increase in $[Chl]_{SAT}$ is observed. The light limitation when MLD is the deepest (January/February) produces a delay between nitrate supplies and consumption, which explains a DeltaMax of 30 days.

[50] In the "No Bloom 1 Ionian" bioregion, P_{rLIGHT} is permanently equal to zero across the whole year (Figure 6d), indicating that for this type of bioregion ("No Bloom"), only the variability of P_{rNUT} could be relevant. P_{rNUT} is close to zero for most of the year, except during winter months (Figure 6b). Although MLD starts to deepen in October (Table 3), it is only in November that we first observe P_{rNUT} values superior to zero, indicating that an efficient, although weak, uptake of nitrates in the surface layers is occurring. The delay in CHL-DateInit compared to MLD-DateInit (DeltaInit $\sim$ 30 days), might be explained by null values of P_{rNUT} before November. Moreover, as light is never limiting, $[Chl]_{SAT}$ cycle follows the P_{rNUT} cycle, with the $[Chl]_{SAT}$ maxima observed concomitantly to the P_{rNUT} maxima. It would explain the DeltaMax low values for the "No Bloom" bioregions. Finally, P_{rNUT} values remain low during winter months (compared to the "Bloom" bioregion, compare Figures 6a and 6b), implying that the nutrient limitation is only episodically relaxed, and also explaining the low values of CHL-Max observed in theses bioregions. In other terms, it is hypothesized that, in spite of a deep MLD in the "No Bloom" bioregions, the position of the nutricline is too deep to allow nutrient accumulation in surface during winter. Only episodic nutrient supplies to the surface seem possible.

[51] It appears that from June to December the two bioregions presented above display similar mechanisms for the regulation of phytoplankton growth. This situation is marked by $P_{rLIGHT} = 0$ and an increase of $[Chl]_{SAT}$ concurrent to the increase of MLD in November/December. One can assume that the progressive increase of $[Chl]_{SAT}$ may be due to the progressive entrainment of subsurface waters (waters close to the nitracline, $0 < P_{rNUT} < 1$), which would increase the carrying capacity of the system. This $[Chl]_{SAT}$ increase clearly corresponds to an "entrainment bloom" as defined by *Cullen et al*. [2002]. In the "No Bloom" bioregion, this "entrainment bloom" persists until water column stratification takes place in March, whereas in the "Bloom" bioregion a decoupling between large nutrients supplies and slow phytoplankton uptake appears in January/February. Subsequently, the important $[Chl]_{SAT}$ increase in March/April in the "Bloom" bioregion corresponds to a "detrainment bloom" as defined by *Cullen et al*. [2002]. The "Detrainment Bloom" occurs when water column stratification is induced in deep mixing layers. Extrapolating these results to the Mediterranean Sea, it appears that the "entrainment bloom" situation is dominant over the basin, whereas the "detrainment bloom" situation should to be considered as an exception.

5. Conclusion

[52] The phytoplankton phenology proves to be an invaluable tool for assessing the extent to which marine ecosystems react to external forcing [*Ji et al*., 2010]. This is particularly true in the Mediterranean Sea, which is considered to be a "hot spot" for the climatic change [*Giorgi*, 2006]. Mediterranean ecosystems could be considered as "sentinels" to anticipate the whole global ocean response to climatic change [*Siokou-Frangou et al*., 2010] and, in this context, phytoplankton phenological indices represent precious information regarding the possible variations induced by environmental conditions. Phenological indices in the ocean can be correlated with an evaluation of the external abiotic forcing, which is primarily represented by MLD dynamics.

[53] To address this topic, a large data set of observations (satellite and in situ) has been assembled to generate, using different averaging methods, concomitant annual MLD and $[Chl]_{SAT}$ cycles. The bioregionalization proposed by DR09 was used as a geographical framework to analyze the available data and maximize their interpretation. To quantitatively analyze MLD and $[Chl]_{SAT}$ time series, several indices were calculated from each annual MLD and $[Chl]_{SAT}$ time series. Specific emphasis was put on the relevance of delta indices.

[54] The coexistence in the Mediterranean Sea of two dominant phenological regimes, named "Bloom" and "No Bloom", was confirmed. The first appears close to what is observed in temperate seas, whereas the second is similar to the regimes of subtropical areas [*Longhurst*, 2006]. It was demonstrated that the MLD plays a key role in determining the phenological cycle (i.e., "Bloom" or "No Bloom"). Furthermore, the two dynamics only diverge between December/January and early summer. In fact, a $[Chl]_{SAT}$ increase was always found to be followed by a MLD deepening in late fall (DeltaInit stable around 30 days) in all regions of the Mediterranean Sea. However, the time lag between MLD and $[Chl]_{SAT}$ peaks (i.e., DeltaMax) diverges between "Bloom" and "No Bloom" regimes. "No Bloom" regime is characterized by concomitant MLD and $[Chl]_{SAT}$ peaks, whereas, in the "Bloom" regime, MLD peak precedes $[Chl]_{SAT}$ peak by about 30 days. This difference points out that the "Bloom" and "No Bloom" bioregions are not exclusively differentiated by the value of $[Chl]_{SAT}$ and MLD annual maxima, but that the date of these events is also relevant.

[55] For the "No Bloom" regime, observations indicate that phytoplankton would never be limited by light, whatever the MLD, and would even grow during the winter period thanks to small nutrient inputs. For the "Bloom" regime, an accumulation of nutrients in surface waters during winter was hypothesized, due to a decoupling between important supplies by deep mixing and a low uptake rate by phytoplankton, which would be episodically limited by a deficit of light. During spring, when both nutrient and light limitations are removed, phytoplankton would exponentially grow. Hence, the "Bloom" regime of the Mediterranean Sea would fit the theoretical model of *Sverdrup* [1953]. According to *Sverdrup* [1953], a bloom begins as soon as the MLD becomes shallower than the critical depth. Even if the *Sverdrup* [1953] theory has been criticized on specific points (i.e., the relative importance of turbulence intensity compared with MLD [*Huisman et al*., 1999; *Taylor and Ferraris*, 2011] or concerning the too simplistic

representation of losses due to respiration in the model [*Smetacek and Passow*, 1990; *Behrenfeld*, 2010]), this theory has been roughly verified in this study with the demonstration that, during certain winters, MLD can be episodically deeper than the critical depth and that phytoplankton growth is limited.

[56] To fully understand the impact of abiotic forcing on phytoplankton phenology, it would be best to observe, continuously and over the whole water column, turbulence, irradiance, nutrient concentration, and phytoplankton biomass. As these variables are not easily measurable, proxies are generally used. Indeed, studies that focus on global ocean or on large oceanic regions generally merged $[Chl]_{SAT}$ with either MLD climatologies [*Obata et al*., 1996; *Wilson and Coles*, 2005] or MLD estimations derived from model [*Henson et al*., 2009; *Chiswell et al*., 2013] or sea surface temperature (SST, used as proxy of MLD [*Volpe et al*., 2012]). In the present study, similarly to *Martinez et al*. [2011] and *Henson et al*. [2006], in situ MLD observations and $[Chl]_{SAT}$ were used. In this context, the Mediterranean Sea, one of the most observed regions of the global ocean, is certainly an ideal place to carry out similar analysis. Nevertheless, the distribution of in situ observations is also sparse over the Mediterranean. Consequently, large geographic units (i.e., the bioregions) and strong averaging procedures had to be used (for the nutrient analysis only climatological analysis over a few bioregions was possible). In consequence, interpretation of the impact of abiotic forcing on phytoplankton phenology was significantly limited. However, this work demonstrates that the synergy between ocean color satellite data and T/S profiles of Argo floats can provide precious information. In this context, it is quite probable that, as already demonstrated on certain specific examples [*Boss et al*., 2008; *Boss and Behrenfeld*, 2010; *Johnson et al*., 2010], time series derived from Argo floats equipped with biogeochemical sensors will strongly improve our interpretation of the mechanisms that control phytoplankton growth.

[57] **Acknowledgments.** The authors thank the U.S. NASA Agency for the easy access to SeaWiFS and MODIS data. We also want to thank the people involved in the collection of the data that are made freely available by the International Argo Project, a pilot program of the Global Ocean Observing System. The European IP SESAME project is thanked for the distribution of nutrients data in the Mediterranean. This work is a contribution to the Remotely Sensed Biogeochemical Cycles in the Ocean (remOcean) project, funded by the European Research Council (grant agreement 246777), to the French "Equipement d'avenir" NAOS project (ANR J11R107-F) and to the European GROOM project. We also thank the GIS COOC (Scientific Interest Group Colour of the Ocean), which contributed to publication costs. We are also grateful to Josephine Ras for reviewing the manuscript, and we thank the two anonymous referees for their constructive comments.

References

Beaugrand, G. (2004), The North Sea regime shift: Evidence, causes, mechanisms and consequences, *Prog. Oceanogr.*, *60*(2–4), 245–262, doi:10.1016/j.pocean.2004.02.018.

Behrenfeld, M. J. (2010), Abandoning Sverdrup's critical depth hypothesis on phytoplankton blooms, *Ecology*, *91*(4), 977–989, doi:10.1890/09–1207.1.

Behrenfeld, M. J., E. Boss, D. A. Siegel, and D. M. Shea (2005), Carbon-based ocean productivity and phytoplankton physiology from space, *Global Biogeochem. Cycles*, *19*, GB1006, doi:10.1029/2004GB002299.

Behrenfeld, M. J., R. T. O'Malley, D. A. Siegel, C. R. McClain, J. L. Sarmiento, G. C. Feldman, A. J. Milligan, P. G. Falkowski, R. M. Letelier, and E. S. Boss (2006), Climate-driven trends in contemporary ocean productivity, *Nature*, *444*(7120), 752–755, doi:10.1038/nature05317.

Bernardello, R., J. G. Cardoso, N. Bahamon, D. Donis, I. Marinov, and A. Cruzado (2012), Factors controlling interannual variability of vertical organic matter export and phytoplankton bloom dynamics—A numerical case-study for the NW Mediterranean Sea, *Biogeosciences*, *9*(11), 4233–4245, doi:10.5194/bg-9–4233-2012.

Bosc, E., A. Bricaud, and D. Antoine (2004), Seasonal and interannual variability in algal biomass and primary production in the Mediterranean Sea, as derived from 4 years of SeaWiFS observations, *Global Biogeochem. Cycles*, *18*, GB1005, doi:10.1029/2003GB002034.

Boss, E., and M. Behrenfeld (2010), In situ evaluation of the initiation of the North Atlantic phytoplankton bloom, *Geophys. Res. Lett.*, *37*, L18603, doi:10.1029/2010GL044174.

Boss, E., D. Swift, L. Taylor, P. Brickley, R. Zaneveld, S. Riser, M. J. Perry and P. G. Strutton (2008), Observations of pigment and particle distributions in the western North Atlantic from an autonomous float and ocean color satellite, *Limnol. Oceanogr.*, *53*(5, Part 2), 2112–2122, doi:10.4319/lo.2008.53.5_part_2.2112.

Brainerd, K. E., and M. C. Gregg (1995), Surface mixed and mixing layer depths, *Deep Sea Res. Part I*, *42*(9), 1521–1543, doi:16/0967-0637(95)00068-H.

Carton, J. A., S. A. Grodsky, and H. Liu (2008), Variability of the oceanic mixed layer, 1960–2004, *J. Clim.*, *21*(5), 1029–1047.

Cermeño, P., S. Dutkiewicz, R. P. Harris, M. Follows, O. Schofield, and P. G. Falkowski (2008), The role of nutricline depth in regulating the ocean carbon cycle, *Proc. Natl. Acad. Sci. U. S. A.*, *105*(51), 20,344–20,349, doi:10.1073/pnas.0811302106.

Chifflet, M., V. Andersen, L. Prieur, and I. Dekeyser (2001), One-dimensional model of short-term dynamics of the pelagic ecosystem in the NW Mediterranean Sea: Effects of wind events, *J. Mar. Syst.*, *30*(1), 89–114.

Chiswell, S. M., J. Bradford-Grieve, M. G. Hadfield, and S. C. Kennan (2013), Climatology of surface chlorophyll a, autumn-winter and spring blooms in the south–west Pacific Ocean, *J. Geophys. Res. Oceans*, *118*, 1003–1018, doi:10.1002/jgrc.20088.

Claustre, H., A. Morel, S. Hooker, M. Babin, D. Antoine, K. Oubelkheir, A. Bricaud, K. Leblanc, B. Quéguiner, and S. Maritorena (2002), Is desert dust making oligotrophic waters greener?, *Geophys. Res. Lett.*, *29*(10), 1469, doi:10.1029/2001GL014056.

Crispi, G., A. Crise, and C. Solidoro (2002), Coupled Mediterranean ecomodel of the phosphorus and nitrogen cycles, *J. Mar. Syst.*, *33–34*, 497–521, doi:10.1016/S0924–7963(02)00073-8.

Cullen, J. (1982), The deep chlorophyll maximum—Comparing vertical profiles of Chlorophyll-A, *Can. J. Fish. Aquat. Sci.*, *39*(5), 791–803.

Cullen, J. J., P. J. Franks S., D. M. Karl, and A. Longhurst (2002), Physical influences on marine ecosystem dynamics, in *The Sea, vol. 12, Ideas and Observations on Progress in the Study of the Seas*, edited by A. R. Robinson, J. J. McCarthy, and B. J. Rothschild, pp. 297–336, John Wiley & Sons, Inc., New York.

D'Ortenzio, F., and M. Ribera d'Alcalà (2009), On the trophic regimes of the Mediterranean Sea: A satellite analysis, *Biogeosciences*, *6*(2), 139–148, doi:10.5194/bg-6–139-2009.

D'Ortenzio, F., and L. Prieur (2010), The upper mixed layer, in *Life in the Mediterranean Sea: A Look at Habitat Changes*, edited by N. Stambler, pp. 127–156, Nova Science Publishers, Inc. New York.

D'Ortenzio, F., S. Marullo, M. Ragni, M. Ribera d'Alcalà, and R. Santoleri (2002), Validation of empirical SeaWiFS algorithms for chlorophyll-a retrieval in the Mediterranean Sea: A case study for oligotrophic seas, *Remote Sens. Environ.*, *82*(1), 79–94, doi:16/S0034–4257(02)00026-3.

D'Ortenzio, F., D. Iudicone, C. Montegut, P. Testor, D. Antoine, S. Marullo, R. Santoleri, and G. Madec (2005), Seasonal variability of the mixed layer depth in the Mediterranean Sea as derived from in situ profiles, *Geophys. Res. Lett.*, *32*, L12605, doi:10.1029/2005GL022463.

D'Ortenzio, F., D. Antoine, E. Martinez and M. Ribera d'Alcalà (2012), Phenological changes of oceanic phytoplankton in the 1980s and 2000s as revealed by remotely sensed ocean-color observations, *Global Biogeochem. Cycles*, *26*, GB4003, doi:10.1029/2011GB004269.

de Boyer Montegut, C., G. Madec, A. Fischer, A. Lazar, and D. Iudicone (2004), Mixed layer depth over the global ocean: An examination of profile data and a profile-based climatology, *J. Geophy. Res.*, *109*, C12003, doi:10.1029/2004JC002378.

Demarcq, H., G. Reygondeau, S. Alvain, and V. Vantrepotte (2012), Monitoring marine phytoplankton seasonality from space, *Remote Sens. Environ.*, *117*, 211–222, doi:10.1016/j.rse.2011.09.019.

Dutkiewicz, S., M. Follows, J. Marshall, and W. W. Gregg (2001), Interannual variability of phytoplankton abundances in the North Atlantic, *Deep Sea Res. Part II*, *48*(10), 2323–2344, doi:16/S0967-0645(00)00178-8.

Fofonoff, N., and J. R. Millard Jr. (1983), Algorithms for computation of fundamental properties of seawater, UNESCO technical papers in marine science, 44, p. 53.

Franz, B. A., P. J. Werdell, G. Meister, S. W. Bailey, R. E. Eplee, G. C. Feldman, E. Kwiatkowskaa, C. R. McClain, F. S. Patt, and D. Thomas (2005), The continuity of ocean color measurements from SeaWiFS to MODIS, in: J.J. Butler (Ed.), *Earth observing systems: X. Proceedings SPIE, vol. 5882*, The International Society for Optical Engineering, pp. 1–13.

Gačić, M., G. Civitarese, S. Miserocchi, V. Cardin, A. Crise, and E. Mauri (2002), The open-ocean convection in the Southern Adriatic: A controlling mechanism of the spring phytoplankton bloom, *Cont. Shelf Res.*, *22*(14), 1897–1908, doi:10.1016/S0278–4343(02)00050-X.

Geider, R. J., H. L. MacIntyre, and T. M. Kana (1997), Dynamic model of phytoplankton growth and acclimation: Responses of the balanced growth rate and the chlorophyll a:carbon ratio to light, nutrient-limitation and temperature, *Mar. Ecol. Prog. Ser.*, *148*(1-3), 187–200, doi:10.3354/meps148187.

Giorgi, F. (2006), Climate change hot-spots, *Geophys. Res. Lett.*, *33*, L08707, doi:10.1029/2006GL025734.

Henson, S. A., I. Robinson, J. T. Allen, and J. J. Waniek (2006), Effect of meteorological conditions on interannual variability in timing and magnitude of the spring bloom in the Irminger Basin, North Atlantic, *Deep Sea Res. Part I*, *53*(10), 1601–1615, doi:10.1016/j.dsr.2006.07.009.

Henson, S. A., J. P. Dunne, and J. L. Sarmiento (2009), Decadal variability in North Atlantic phytoplankton blooms, *J. Geophys. Res.*, *114*, C04013, doi:10.1029/2008JC005139.

Huisman, J., P. van Oostveen, and F. J. Weissing (1999), Critical depth and critical turbulence: Two different mechanisms for the development of phytoplankton blooms, *Limnol. Oceanogr.*, *44*(7), 1781–1787.

Ignatiades, L., O. Gotsis-Skretas, K. Pagou, and E. Krasakopoulou (2009), Diversification of phytoplankton community structure and related parameters along a large-scale longitudinal east–west transect of the Mediterranean Sea, *J. Plankton Res.*, *31*(4), 411–428.

Ji, R., M. Edwards, D. L. Mackas, J. A. Runge and C. A. Thomas (2010), Marine plankton phenology and life history in a changing climate: Current research and future directions, *J. Plankton Res.*, *32*(10), 1355–1368, doi:10.1093/plankt/fbq062.

Johnson, K. S., S. C. Riser, and D. M. Karl (2010), Nitrate supply from deep to near-surface waters of the North Pacific subtropical gyre, *Nature*, *465*(7301), 1062–1065, doi:10.1038/nature09170.

Lacroix, G., and M. Grégoire (2002), Revisited ecosystem model (MODECOGeL) of the Ligurian Sea: Seasonal and interannual variability due to atmospheric forcing, *J. Mar. Syst.*, *37*(4), 229–258, doi:10.1016/S0924–7963(02)00190-2.

Lazzari, P., C. Solidoro, V. Ibello, S. Salon, A. Teruzzi, K. Béranger, S. Colella, and A. Crise (2012), Seasonal and inter-annual variability of plankton chlorophyll and primary production in the Mediterranean Sea: A modelling approach, *Biogeosciences*, *9*(1), 217–233, doi:10.5194/bg-9–217-2012.

Lévy, M., L. Mémery, and J.-M. André (1998), Simulation of primary production and export fluxes in the Northwestern Mediterranean Sea, *J. Mar. Res.*, *56*(1), 197–238.

Longhurst, A. R. (2006), *Ecological Geography of the Sea*, 2nd ed., Academic Press, Burlington, Mass.

Mann, K. H., and J. R. N. Lazier (2006), *Dynamics of Marine Ecosystems: Biological-Physical Interactions in the Oceans*, Wiley-Blackwell, Malden, Mass.

Maillard, C., et al. (2002), An integrated system for managing multidisciplinary oceanographic data collected in the Mediterranean Sea during the basin-scale research project EU/MAST-MATER (1996–2000), *J. Mar. Syst.*, *33–34*, 523–538, doi:10.1016/S0924–7963(02)00074-X.

Maillard, C., et al. (2005), MEDAR/MEDATLAS 1998–2001: A Mediterranean and Black Sea oceanographic data base and network, *Boll. Geofis. Teor. Appl.*, *46*, 329–344.

Martinez, E., D. Antoine, F. D'Ortenzio, and C. de Boyer Montégut (2011), Phytoplankton spring and fall blooms in the North Atlantic in the 1980s and 2000s, *J. Geophys. Res.*, *116*, C11029, doi:10.1029/2010JC006836.

Marty, J.-C., J. Chiavérini, M.-D. Pizay, and B. Avril (2002), Seasonal and interannual dynamics of nutrients and phytoplankton pigments in the western Mediterranean Sea at the DYFAMED time-series station (1991–1999), *Deep Sea Res. Part II*, *49*(11), 1965–1985, doi:16/S0967-0645(02)00022-X.

McClain, C. R., S. R. Signorini, and J. R. Christian (2004), Subtropical gyre variability observed by ocean-color satellites, *Deep Sea Res. Part II*, *51*(1–3), 281–301, doi:10.1016/j.dsr2.2003.08.002.

Menzel, D. W., and J.H. Ryther (1959), The annual cycle of primary production in the Sargasso Sea off Bermuda, *Deep Sea Res.*, *6*, 351–367, doi:10.1016/0146–6313(59)90095-4.

Moutin, T., and P. Raimbault (2002), Primary production, carbon export and nutrients availability in western and eastern Mediterranean Sea in early summer 1996 (MINOS cruise), *J. Mar. Syst.*, *33-34*, 273–288, doi:10.1016/S0924–7963(02)00062-3.

Napolitano, E., T. Oguz, P. Malanotte-Rizzoli, A. Yilmaz, and E. Sansone (2000), Simulations of biological production in the Rhodes and Ionian basins of the eastern Mediterranean, *J. Mar. Syst.*, *24*(3–4), 277–298, doi:10.1016/S0924–7963(99)00090-1.

Obata, A., J. Ishizaka, and M. Endoh (1996), Global verification of critical depth theory for phytoplankton bloom with climatological in situ temperature and satellite ocean color data, *J. Geophys. Res.*, *101*(C9), 20,657–20,667, doi:10.1029/96JC01734.

O'Reilly, J. E., et al. (2000), Ocean color chlorophyll a algorithms for SeaWiFS, OC2, and OC4: version 4, in *SeaWiFS Postlaunch Calibration and Validation Analyses: Part 3*, vol. *11*, edited by S. B. Hooker and E. R. Firestone, pp. 9–23, NASA Goddard Space Flight Center, Greenbelt, Md. and SAIC General Sciences Corporation, Beltsville, Md.

Platt, T., G. N. White, L. Zhai, S. Sathyendranath, and S. Roy (2009), The phenology of phytoplankton blooms: Ecosystem indicators from remote sensing, *Ecol. Modell.*, *220*(21), 3057–3069, doi:10.1016/j.ecolmodel.2008.11.022.

Polovina, J. J., E. A. Howell, and M. Abecassis (2008), Ocean's least productive waters are expanding, *Geophys. Res. Lett.*, *35*, L03618, doi:10.1029/2007GL031745.

Pujo-Pay, M., P. Conan, L. Oriol, V. Cornet-Barthaux, C. Falco, J.-F. Ghiglione, C. Goyet, T. Moutin, and L. Prieur (2011), Integrated survey of elemental stoichiometry (C, N, P) from the western to eastern Mediterranean Sea, *Biogeosciences*, *8*(4), 883–899, doi:10.5194/bg-8–883-2011.

Racault, M.-F., C. Le Quéré, E. Buitenhuis, S. Sathyendranath, and T. Platt (2012), Phytoplankton phenology in the global ocean, *Ecol. Indicators*, *14*(1), 152–163, doi:10.1016/j.ecolind.2011.07.010.

Ribera d'Alcalà, M., G. Civitarese, F. Conversano, and R. Lavezza (2003), Nutrient ratios and fluxes hint at overlooked processes in the Mediterranean Sea, *J. Geophys. Res.*, *108*(C9), 8106, doi:10.1029/2002JC001650.

Rochford, P., A. Kara, A. Wallcraft, and R. Arnone (2001), Importance of solar subsurface heating in ocean general circulation models, *J. Geophys. Res.*, *106*(C12), 30,923–30,938.

Siegel, D. A., S. C. Doney, and J. A. Yoder (2002), The North Atlantic spring phytoplankton bloom and Sverdrup's critical depth hypothesis, *Science*, *296*(5568), 730–733, doi:10.1126/science.1069174.

Siokou-Frangou, I., U. Christaki, M. G. Mazzocchi, M. Montresor, M. Ribera d'Alcalá, D. Vaqué, and A. Zingone (2010), Plankton in the open Mediterranean Sea: A review, *Biogeosciences*, *7*(5), 1543–1586, doi:10.5194/bg-7–1543-2010.

Smetacek, V., and U. Passow (1990), Spring bloom initiation and Sverdrup's critical-depth model, *Limnol. Oceanogr.*, *35*(1), 228–234.

Somot, S., F. Sevault, and M. Déqué (2006), Transient climate change scenario simulation of the Mediterranean Sea for the twenty-first century using a high-resolution ocean circulation model, *Clim. Dyn.*, *27*(7-8), 851–879, doi:10.1007/s00382-006-0167-z.

Sverdrup, H. U. (1953), On conditions for the vernal blooming of phytoplankton, *ICES J. Mar. Sci.*, *18*, 287–295.

Taylor, J. R., and R. Ferrari (2011), Shutdown of turbulent convection as a new criterion for the onset of spring phytoplankton blooms, *Limnol. Oceanogr.*, *56*(6), 2293–2307.

Volpe, G., R. Santoleri, V. Vellucci, M. Ribera d'Alcalà, S. Marullo, and F. D'Ortenzio (2007) The colour of the Mediterranean Sea: Global versus regional bio-optical algorithms evaluation and implication for satellite chlorophyll estimates, *Remote Sens. Environ.*, *107*(4), 625–638, doi:10.1016/j.rse.2006.10.017.

Volpe, G., B. B. Nardelli, P. Cipollini, R. Santoleri, and I. S. Robinson (2012), Seasonal to interannual phytoplankton response to physical processes in the Mediterranean Sea from satellite observations, *Remote Sens. Environ.*, *117*, 223–235, doi:10.1016/j.rse.2011.09.020.

Wilson, C., and V. J. Coles (2005), Global climatological relationships between satellite biological and physical observations and upper ocean properties, *J. Geophys. Res.*, *110*, C10001, doi:10.1029/2004JC002724.

Yoder, J. A., C. R. McClain, G. C. Feldman, and W. E. Esaias (1993), Annual cycles of phytoplankton chlorophyll concentrations in the global ocean: A satellite view, *Global Biogeochem. Cycles*, *7*(1), 181–193, doi:10.1029/93GB02358.